Catalysis Today 175 (2011) 55–64

Contents lists available at ScienceDirect

Catalysis Today

journal homepage: www.elsevier.com/locate/cattod

Nanofibrous Pt-Ba Lean NO_x trap catalyst with improved sulfur resistance and thermal durability

I.S. Pieta[a,b], W.S. Epling[b,*], M. García-Diéguez[a], J.Y. Luo[b], M.A. Larrubia[a], M.C. Herrera[a], L.J. Alemany[a,**]

[a] Department of Chemical Engineering, Faculty of Science, University of Malaga, Campus of Teatinos, 29071, Malaga, Spain
[b] Department of Chemical Engineering, University of Waterloo, Waterloo, Ontario, N2L 3G1, Canada

ARTICLE INFO

Article history:
Received 19 October 2010
Received in revised form 28 January 2011
Accepted 26 February 2011
Available online 8 April 2011

Keywords:
NO_x storage
Pt-Ba/Al_2O_3
Thermal durability
Sulfur resistance

ABSTRACT

Different LNT catalysts, prepared using γ-Al_2O_3, nanofibrous Al_2O_3 and TiO_2-modified nanofibrous Al_2O_3 supports, with Ba as the storage component and Pt as the oxidation component, have been prepared and NO_x uptake behaviour was examined between 523 and 823 K. The activity study was accompanied by TEM, XRD and H_2 chemisorption characterization. The Pt-Ba nanofibrous Al_2O_3-supported catalyst resulted in the best performance, likely due to better Pt dispersion. This included improved storage capacity as well as more efficient reduction during the regeneration phase. This catalyst also had better performance after identical S exposures and after desulfurization. Ti modification had significant impact on sample thermal durability and general catalyst performance. Results using the Al_2O_3-TiO_2 nanofibrous catalyst reveal that this catalyst has improved thermal degradation resistance properties relative to standard γ-Al_2O_3. Ti incorporation in the nanofibrous Al structure was found to also promote sulfur desorption. Above 1073 K, where complex $Ba_xTi_yO_z$, and/or $Ba_xAl_yTi_zO_n$ structures form, the Ba-Ti interaction was found to have a destabilizing effect on stored nitrites/nitrates.

1. Introduction

NO_x storage/reduction catalysts (NSR or lean NO_x trap – LNT) are being investigated and used to meet current and forthcoming Euro and EPA emission standards for lean-burn engines [1–6]. Since the NSR principle was first reported by Toyota [3,7,8], a large number of studies investigating various NSR catalysts have been published [6,9–12]. One of the most commonly studied NSR catalyst compositions is the Pt-Ba system supported on γ-Al_2O_3, as first discussed by Toyota [12–14]. Many studies have been performed with such a standard formulation; Pt:AE:Al_2O_3 ≈ 1:20:100 (AE – alkali or alkaline earth element); however, there is still a need to improve the catalyst's thermal durability and sulfur tolerance, which are primary drawbacks of the NSR catalysts, hindering more widespread commercial application [15].

NSR catalysts normally operate in the 473–673 K temperature range. Above this temperature, the NO_x storage capacity is limited by thermal stability of the trapped nitrites/nitrates [12,16,17]. However, during normal engine operation some event may provoke a sudden, uncontrolled increase in temperature along the catalyst, i.e. combustion of soot accumulated in a diesel particulate filter (DPF) placed upstream with respect to the NSR catalyst, increasing the exhaust gas temperature to induce the onset of soot oxidation if the DPF is downstream, or simply high torque driving conditions. However, due to S accumulation on an NSR catalyst, intermittent high temperature exposure is also required to regenerate the catalyst, i.e. remove the S species for regenerated efficiency. In order to induce S release, the working temperature of the catalyst needs to exceed 873 K for most formulations. Previous data indicate that the high temperatures required for desulfurization result in thermal degradation of NO_x traps [18,19]. Thermal degradation includes precious metal sintering [20,21], trapping material sintering [13], as well as reaction between the trapping material and alumina support [13,18]. Despite the continuous reduction in sulfur concentration in refined fuels and modifications in NSR catalyst formulations, which often target improved sulfur tolerance, sulfur poisoning remains a key issue in NSR application [2,22–25]. Taking into account the stability of sulfates on the NSR trapping component, new NSR formulations need to be developed that are more S resistant or release S at lower temperatures. As an added complication, although not required, when S is released from the catalyst under rich conditions, H_2S formation would be undesired due to the associated odor at rather low concentrations. Furthermore, new formulations that preserve trapping efficiencies at high temperatures would expand their applicability as well as maintain NO_x removal performance during desulfurization events [26].

* Corresponding author.
** Corresponding author. Fax: +34 952131919.
E-mail addresses: wepling@uwaterloo.ca (W.S. Epling), luijo@uma.es (L.J. Alemany).

0920-5861/$ – see front matter © 2011 Elsevier B.V. All rights reserved.
doi:10.1016/j.cattod.2011.02.045

There are a few studies directed at high-temperature NSR catalysts, and the possible reactions that may occur between the NO_x storage compound and support at high temperatures, e.g., $BaO + Al_2O_3 \rightarrow BaAl_2O_4$ [26–29]. Enhanced NO_x storage capacity at high temperature has been reported for a Pt-K/$MgAl_2O_4$ catalyst [30]. A novel Pt/$K_2Ti_2O_5$ catalyst has also been reported as a high-temperature NSR catalyst [26]. It was found that the adsorbed NO_x on Pt/$K_2Ti_2O_5$ was much more stable than that trapped over Pt-K/TiO_2. Mechanistic studies revealed that KNO_3-like compounds were formed after NO_x adsorption, and that the NO_x storage and reduction process on $K_2Ti_2O_5$ was accompanied by a structural transformation between $K_2Ti_2O_5$ and $K_2Ti_6O_{13}$. Although K as the trapping component can result in considerable NO_x storage capacity, and TiO_2 is accepted as relatively resistant to sulfur poisoning [12,31], previous studies report better performance using a Ba-based rather than the K-based NSR catalyst [12,31].

In this study, the activity of a novel nanofibrous Pt-Ba/Al_2O_3 catalyst for NO_x removal at high temperature is reported. The aim of the present work is the development of a thermally stable NSR catalyst supported on γ-Al_2O_3 modified with additional components, which may also increase the sulfur tolerance of the material.

2. Materials and methods

2.1. Catalyst preparation and characterization

Synthesized nanostructured γ-Al_2O_3 (denoted Al_{NF}) and nanostuctured γ-Al_2O_3-TiO_x (denoted Al-Ti) were used as supports. The preparation procedure has been described in detail elsewhere [32,33]. An aqueous $NaAlO_2$ solution was added dropwise to a 5 N acetic acid solution. The obtained precipitate was decanted, filtered and washed with water. The resulting powder was dried overnight at 373 K and subsequently mixed with a non-ionic surfactant, Tergitol (15-TS-5, Sigma), using a Tergitol/Al ratio of 0.5. The mixture was kept in an autoclave for 72 h at 373 K and later calcined at 773 K for 20 h. The same preparation procedure was applied to obtain nanostructured Al-Ti, but with the addition of $TiCl_3$ as a precursor (12% $TiCl_3$ in hydrochloric acid, Sigma). Both, Al- and Ti-precursors were added dropwise simultaneously to the acetic acid solution. The Tergitol/(Al + Ti) ratio was 0.5. The autoclaved mixture was calcined at 623 K for 2 h and the temperature was then increased at 5 K min^{-1} to 773 K and maintained at 773 K for 18 h. In case of sample treated at 1073 K or 1273 K, the additional calcination was performed with a previous calcined catalyst sample for 1 h.

The Pt and Ba components were added via the incipient wetness impregnation method using diamminedinitroplatinum (II) ($Pt(NH_3)_2(NO_2)_2$, Aldrich) and barium acetate ($Ba(CH_3COO)_2$, MERCK) as precursors. The catalyst formulations are summarized in Table 1. The metal loading is expressed as formal surface atomic density (atoms per nanometer square, at nm^{-2}) for comparison in terms of surface coverage. First Pt (0.4 at nm^{-2}; 0.4Pt/Al_{NF}, 0.4Pt/Al-Ti) catalysts were prepared by impregnation of the Al_{NF} and Al-Ti supports with an aqueous solution of Pt, drying overnight at room temperature and calcination for 3 h at 648 K in air. These were then impregnated with Ba (4 at nm^{-2} of Ba) to obtain the final formulations (0.4Pt-4Ba/Al_{NF}, 0.4Pt-4Ba/Al-Ti). The final calcination was performed for 5 h at 798 K in air.

The Pt-Ba/Al-Ti_{MF} physical mixture was prepared by mixing the prepared 0.4Pt-4Ba/Al_{NF} catalyst with rutile TiO_2 powder (Sigma–Aldrich, 99.7% purity, used as received) in a 9:1 ratio. The standard Pt-Ba/Al_2O_3 catalyst, denoted as Pt-Ba_{ST}, has been described in detail elsewhere along with its preparation procedure [12].

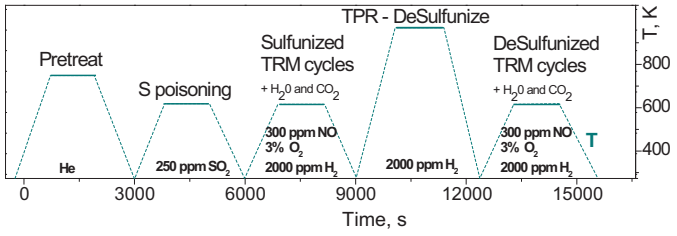

Fig. 1. S poisoning experiment scheme.

The TEM images of powder samples deposited onto a copper mesh grid coated with a carbon film were taken with a Philips CM200 (200 kV) microscope equipped with an EDX (energy dispersive X-ray) detector. The XRD patterns of the powder samples were recorded with a Siemens D-501 goniometer equipped with a Johansson type monochromator with a Ge(111) crystal. During measurement, Cu Kα1 radiation and a fixed power source (45 kV and 35 mA) were used.

N_2 adsorption–desorption isotherms for the Al_{NF} and Al-Ti supports were obtained at 77 K using a Beckman Coulter SA3100 Surface Area Analyzer. Before the analysis, the samples were outgassed in vacuum (1×10^{-3} Pa) for 5 h at 453 K. The specific surface area was obtained by the BET isotherm equation and the pore volume by the Barrett–Joyner–Halenda (BJH) method from the desorption branch of the isotherm.

H_2 chemisorption experiments were carried out in the pulse mode in a Hiden CATLAB microreactor module connected to a Hiden QIC-20 gas analysis system. Prior to H_2 chemisorption, each sample was heated from room temperature (RT) to 723 K in the presence of H_2 (5% H_2 in He). The sample was then reduced in this mixture at 723 K for 30 min, and then purged in a He flow. Next, the temperature was decreased to RT and the chemisorption measurements were performed at ca. 310 K. For each experiment, 27 pulses of H_2-containing gas were injected into the reactor (100 μl of 5% H_2 in He each pulse). For calculation purposes, a stoichiometry relation of two platinum sites per one H_2 molecule was used [34].

2.2. Transient response method (TRM)

TRM runs were performed in a quartz tube reactor connected to a Pfeiifer Prisma™ QMS 200 mass spectrometer or in a CATLAB microreactor module connected to a Hiden QIC-20 gas analysis system. The method was used to study the NO_x storage–reduction process over the catalysts between 473 and 773 K with a total gas flow of 100 ml min^{-1} using 60 or 40 mg of catalyst (GHSV = 1.5×10^5 (or 1×10^5) h^{-1}, at 1 atm and 293 K). A rectangular pulse of NO (1000 ppm or 300 ppm) + O_2 (3%) in He flow followed by a H_2 (2000 ppm) in He flow were fed during the oxidation and reduction steps, respectively. For experiments with H_2O and CO_2, 2.5% H_2O and 5% CO_2 were continuously fed to the microreactor. For all experiments, the N-balance closed with a deviation between 4% and 5%.

2.3. Sulfur poisoning study

The sulfur poisoning study was performed in the CATLAB microreactor system. The general experiment scheme is presented in Fig. 1. First, catalyst sulfation was carried out at 623 K for 30 min with a gas mixture containing 250 ppm SO_2, 5% O_2 and a He balance. Then the catalyst was cooled to RT in He and afterwards NO_x storage–reduction measurements and analysis of sulfur-poisoned catalysts were performed using a conventional TRM protocol. The content of H_2O and CO_2 in the gas stream during TRM cycles was 2.5 and 5%, respectively. Next, temperature-programmed reduction

Table 1
Catalyst formulation details (NF – nanofibrous, MF – physical mixture).

Catalyst	Description	Pt (wt.%)	Ba (wt.%)	Al_2O_3 (wt.%)	TiO_2 (wt.%)
0.4Pt-4Ba/γ-Al_2O_3 [12]	Pt-Ba_{ST}	2	20	78	–
γ-$Al_2O_{3\,NF}$	Al_{NF}	–	–	100	–
0.4Pt-4Ba/γ-$Al_2O_{3\,NF}$	Pt-Ba/Al_{NF}	3.8	25	71.2	–
γ-Al_2O_3-$TiO_{2\,NF}$	Al-Ti	–	–	90	10
0.4Pt-4Ba/γ-Al_2O_3-$TiO_{2\,NF}$	Pt-Ba/Al-Ti	2.3	20	69.9	7.8
0.4Pt-4Ba/γ-$Al_2O_{3\,NF}$ + $TiO_{2\,MF}$	Pt-Ba/Al-Ti_{MF}	2.3	20	69.9	7.8

(TPR) was performed. The catalyst was desulfurized in rich conditions (2000 ppm H_2 in He) while ramping from RT to 1023 (or 923) K and afterwards NO_x conversion was evaluated.

3. Results and discussion

3.1. Catalyst characterization

The properties of Pt-Ba_{ST} have been described in detail elsewhere [12]. The measured specific surface area (A_{BET}) and pore volume (V_p) of the pure Al_{NF} support were 300 $m^2\,g^{-1}$ and 1 $cm^3\,g^{-1}$, respectively. For the Al-Ti support, A_{BET} = 160 $m^2\,g^{-1}$ and V_p = 0.4 $cm^3\,g^{-1}$. TEM images of the fresh Al_{NF} and Al-Ti supports and also Pt-Ba/Al_{NF}, Pt-Ba/Al-Ti and Pt-Ba/Al-Ti_{MF} catalysts before the TRM tests are shown in Fig. 2. For both the Al_{NF} and Al-Ti supports, a nanofibrous structure was obtained (Fig. 2a and c). For Pt-Ba/Al_{NF}, Pt-Ba/Al-Ti and Pt-Ba/Al-Ti_{MF} catalysts (Fig. 2b, d, and e), several types of crystallites are observed. The nanofibers correspond to the Al or Al-Ti phase, while bulky, massive crystallites of Ba carbonate are also present. In general, for the Pt-Ba/Al-Ti catalyst, Ti is well incorporated in the Al nanofibers, however, some spherical crystallites corresponding to TiO_2 were detected. The round-like, dark crystallites correspond to Pt (the presence of Pt was also detected by EDX analysis performed during the TEM study). In contrast, TiO_2 (rutile) is present as well-shaped spheres with lower dark contrast, which are clearly seen for Pt-Ba/Al-Ti_{MF} (Fig. 2e). For all prepared materials, Pt forms rather small particles; however, there is no homogeneity in the particle size. Some large Pt crystallites, ca. 20–30 nm, can also be observed (Fig. 2b and d). The average Pt size diameter was ca. 5 and 12 nm for the Pt-Ba/Al_{NF} and Pt-Ba/Al-Ti samples, respectively. The dispersion of Pt for those catalysts was 37 and 18%. The Pt dispersion of Pt-Ba_{ST} was ca. 20%.

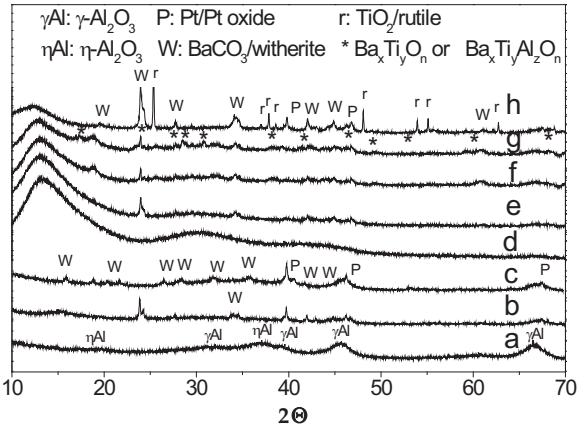

Fig. 3. XRD patterns of the materials after being calcined at 1073 K; (a) Al_{NF}, (b) Pt-Ba/Al_{NF} BR, (c) Pt-Ba/Al_{NF} AR, (d) Al-Ti, (e) Pt-Ba/Al-Ti BR, (f) Pt-Ba/Al-Ti AR, (g) Pt-Ba/Al-Ti calcined at 1273 K and (h) physical mixture of Pt-Ba/Al-Ti_{MF} BR. TRM conditions – 1000 ppm of NO_x + 3% of O_2 in He, T = 623 K.

The XRD patterns obtained from the Al_{NF} and Al-Ti supports and also Pt-Ba/Al_{NF}, Pt-Ba/Al-Ti and Pt-Ba/Al-Ti_{MF} catalysts before (BR) and after reaction (AR) are presented in Fig. 3. Diffractograms from

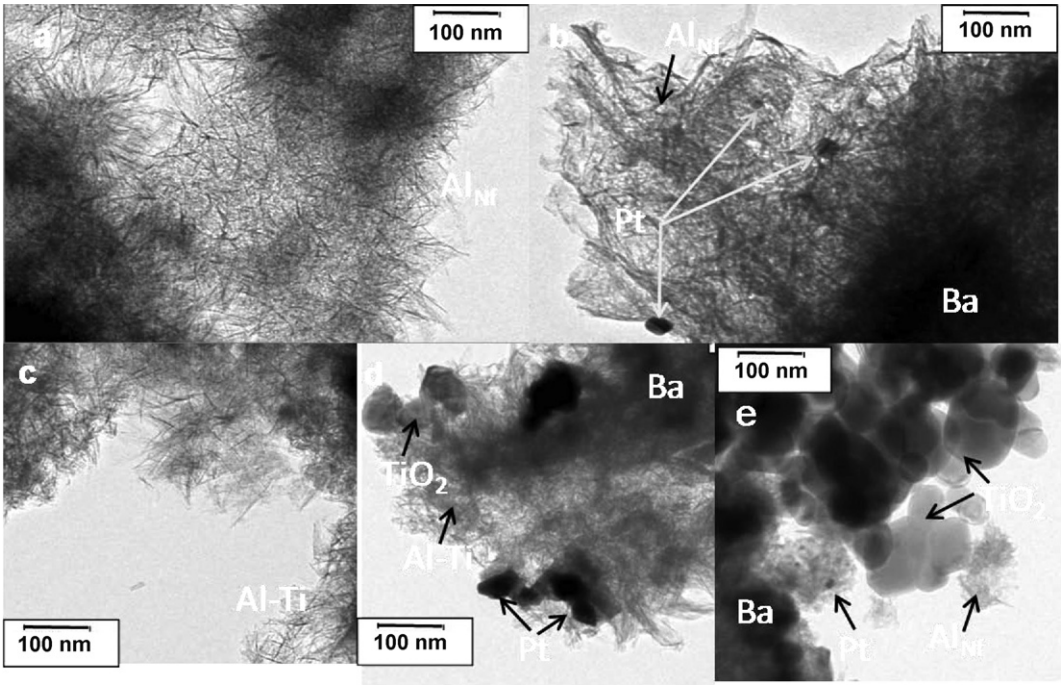

Fig. 2. TEM images of (a) Al_{NF} nanofiber support, (b) Pt-Ba/Al_{NF}, (c) Al-Ti nanofiber support, (d) Pt-Ba/Al-Ti and (e) the physical mixture of Pt-Ba/Al-Ti_{MF}.

both supports (Fig. 3a and d) have the characteristic γ-alumina signals (JCPDS 75-0921). Additionally, for Al-Ti a broad feature in the low 2θ region was detected, which corresponds to very small crystallite sizes of the nanofiber structure. Peaks related to Pt and PtO (JCPDS 70-2431 and JCPDS 83-1997), were detected to only some extent, because these signals are in most cases overshadowed by intense γ-alumina features. For the Ba-containing samples, witherite ($BaCO_3$ JCPDS 5-0378) was the Ba-dominant phase both before and after TRM tests. The XRD data revealed that most likely two Ba species are present on the calcined catalysts. Some of the Ba is probably not detected by XRD indicating high Ba dispersion on the catalysts, which has been described previously as a 'monolayer' [35,36]. For fresh Pt-Ba/Al_{NF} and Pt-Ba/Al-Ti_{MF} catalysts before reaction only a fraction of Ba forms the XRD detected bulk $BaCO_3$ phase. For the Pt-Ba/Al-Ti catalyst, both before and after reaction, an intense signal at $\theta = 24.1^\circ$ and several other peaks in the higher 2θ region, associated with an orthorhombic $BaCO_3$ phase (witherite), indicate large Ba-carbonate crystal formation. These results are in line with previous studies, where the different Ba species on the surface of similar catalysts have been reported [37,38]. The rutile phase (JCPDS 78-2485) was only clearly observed in the case of Pt-Ba/Al-Ti_{MF}.

The comparison of XRD patterns of the BR and AR catalysts suggests that some structural changes occur during the TRM tests. It is worth noting that the Pt-Ba/Al-Ti sample changes less compared to the Pt-Ba/Al_{NF}, which suggests that the Al-Ti support results in better thermal durability than Al_{NF}, thereby preventing thermally induced material changes and Pt sintering. In general, for Ba-containing samples after reaction, multiple peaks in the whole XRD pattern range indicate the presence of the witherite phase. It is also worth pointing out that for Pt-Ba/Al-Ti (Fig. 3e–g) there were no peaks detected which indicate interaction between Ba and Ti phases at temperatures below exposure at 873 K, in agreement with previous observations [39]. However, such an interaction was observed when the Pt-Ba/Al-Ti catalyst was exposed to temperatures higher than 1073 K, with an example of data obtained after calcining at 1273 K shown in Fig. 3g. In terms of K-containing systems, this kind of interaction between Ti and the alkali-phase was observed previously, where the full transformation into potassium titanate was observed after sample treatment at 1123 K for 10 h [26]. In contrast, for the Ba-based system this transformation starts at a slightly lower temperature.

For the samples after reaction, Pt became easier to detect, probably due to Pt sintering and bigger cluster formation, especially for Pt-Ba/Al_{NF}. For the Pt-Ba/Al-Ti catalyst, the initially good dispersion of Pt remains unchanged at TRM conditions up to 873 K. Maintaining the good dispersion implies maintaining the proximity of the Pt sites to alkali metal, which would also maintain high NO_x storage [12]. In accordance with the broadly accepted storage model, i.e., the nitrites/nitrates route [12,40,41], nitrites are progressively transformed into barium nitrates during $NO + O_2$ admission with Pt participation [41]. The same behaviour was observed for a Pt-Ca/Al_2O_3 catalyst [42], and BaO/Al_2O_3 and Pt-BaO/Al_2O_3 catalysts [43]. Small Pt particles can be beneficial for NO_x storage in terms of Pt and the NO_x storage component proximity. However, a too high Pt dispersion is not always desirable for NSR reactivity, since smaller Pt crystallites are more easily oxidized relative to bigger ones in the presence of O_2, and although the overall conversion may increase with better dispersion, on a per exposed atom basis (TOF) NO oxidation will decrease [13].

3.2. Catalytic performance study

NO_x storage–reduction over the Pt-Ba_{ST}, Pt-Ba/Al_{NF}, Pt-Ba/Al-Ti and Pt-Ba/Al-Ti_{MF} catalysts was studied at room temperature, 523, 623, 723 and 773 K, and results obtained over several cycles at 623 K are shown in Fig. 4. These experiments were carried out under H_2O- and CO_2-free conditions to estimate the potential accumulation capacity and NO oxidation over the standard and modified catalyst structures. The results were obtained after conditioning the catalyst at the same temperature with 5 adsorption-reduction cycles. A CO_2 signal was not observed, suggesting that either the $BaCO_3$ phase was fully decomposed during conditioning, leaving BaO and $Ba(OH)_2$ on the surface [13], or that some remained stable, but did not take part in the reaction, i.e. any $BaCO_3$ was unreactive under the conditions tested. For Pt-Ba_{ST}, upon NO admission to the lean phase at $t = 0$ min, a dead time in NO outlet concentration was observed, indicating that all inlet NO_x during that time was completely stored on the catalyst surface. After ca. 0.7 min the NO_x outlet concentration began gradually increasing with time, ultimately reaching the inlet concentration value of 1000 ppm at the end of the 30-min lean/adsorption phase. The NO_2 concentration gradually increased with time and at the end of the cycle was ca. 320 ppm. Compared to Pt-Ba_{ST}, different NO_2 outlet concentrations were detected for Pt-Ba/Al_{NF}, Pt-Ba/Al-Ti and Pt-Ba/Al-Ti_{MF} at the end of lean phase; 390, 45 and 160 ppm, respectively (Fig. 4b–d). For the Pt-Ba/Al-Ti sample, this low NO oxidation activity can be related to the Pt-TiO_2 electron interaction as was pointed out previously [44]. It was found that a Pt-TiO_2 catalyst prepared by impregnation contains Pt metallic species and PtO, which is less active than metallic Pt, so exhibits low NO oxidation activity. Additionally, small Pt clusters on TiO_2 with weak Pt-TiO_2 electron interaction are easily oxidized during reaction under oxidizing conditions, leading to a decrease in NO oxidation activity [45]. Considering the Pt-Ba/Al-Ti_{MF} physical mixture, the Pt-TiO_2 electron interaction is expected to be weaker compared to that for Pt-Ba/Al-Ti. Because of that, the NO oxidation activity is greater for Pt-Ba/Al-Ti_{MF} compared to Pt-Ba/Al-Ti. Although the Pt-Ba/Al_{NF} sample had the highest dispersion, it also resulted in the best NO oxidation activity. This simply indicates that the higher level of Pt exposed led to a higher rate, although the TOF would be smaller [13].

The NO breakthrough time for both the Pt-Ba/Al-Ti and Pt-Ba/Al-Ti_{MF} catalysts also decreased, to less than 10–15 s. In the case of Pt-Ba/Al_{NF} the NO breakthrough time increased by ca. 20% compared to Pt-Ba_{ST}. It is well known that NO to NO_2 oxidation plays a key role for NO_x storage [11,13] and the changes in breakthrough time correlate well to the NO oxidation ability of the catalysts. The higher the NO_2 outlet concentration at the end of the lean phase, the longer the storage occurred. It is also possible that the different overall performances, as well as the NO oxidation ability, are due to different crystallinity and dispersion states of the Ba phase. In the case of Pt-Ba/Al-Ti, large crystals of $Ba(NO_3)_2$ form the large $BaCO_3$ crystals shown in Fig. 2, and the large nitrate crystals were also observed with TEM after reaction as well (data not shown), which can evoke NO_x diffusion/mobility difficulty during storage. For Pt-Ba/Al_{NF}, the Ba phase is more dispersed and could form smaller crystallites, which is beneficial for NO_x storage capacity [46,47].

At 623 K, Pt-Ba/Al_{NF} had the highest accumulation capacity of the samples tested. The amounts of stored nitrates at 623 K for Pt-Ba_{ST}, Pt-Ba/Al_{NF} and Pt-Ba/Al-Ti were 1.26×10^{-3}, 1.57×10^{-3} and 9.93×10^{-4} mol g_{cat}^{-1}, respectively. For the physical mixture, Pt-Ba/Al-Ti_{MF}, the amount of NO_x stored was ca. 1.17×10^{-3} mol g_{cat}^{-1}, and falls between the values obtained for Pt-Ba/Al_{NF} and Pt-Ba/Al-Ti. These values were estimated taking into account that the amount of stored nitrates is proportional to the area A_1 in Fig. 4.

In terms of regeneration, also in Fig. 4, for Pt-Ba_{ST} H_2 was completely consumed for about 3 min after its introduction at $t = 25$ min. Then the H_2 outlet concentration gradually increased with time, reaching the inlet value at the end of the rich step at ca. 55 min. N_2 was observed at the onset of the rich phase, suggesting fast reduction of stored nitrites/nitrates. H_2O was also observed at the onset of the regeneration phase, via reaction between H_2 and the stored NO_x

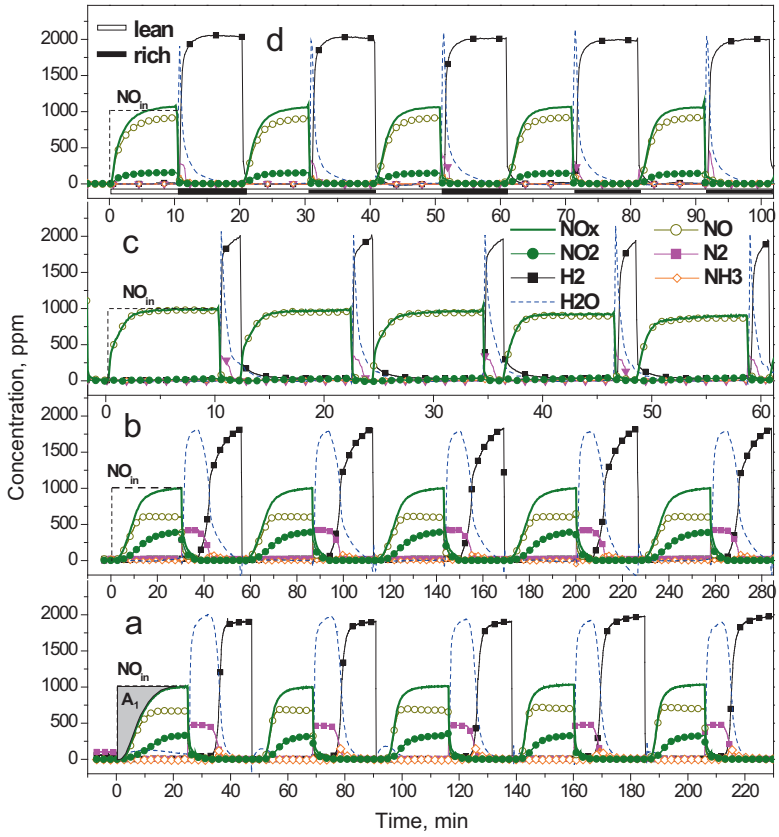

Fig. 4. Storage–reduction of NO_x at 623 K for (a) Pt-Ba_{ST}, (b) Pt-Ba/Al_{NF}, (c) Pt-Ba/Al-Ti and (d) the physical mixture of Pt-Ba/Al-Ti_{MF}. Lean phase – 1000 ppm NO_x + 3% of O_2 in He; regeneration phase – 2000 ppm H_2 in He. Gas flow = 100 ml min^{-1}.

species. After 38 min, while N_2 and H_2O concentrations decreased and H_2 approached the inlet concentration, NH_3 was observed, ca. 130 ppm at its peak. Complete H_2 consumption over both Pt-Ba/Al-Ti and Pt-Ba/Al-Ti_{MF} catalysts was shorter compared to Pt-Ba_{ST} and Pt-Ba/Al_{NF}; less than 0.5 min, and shorter H_2O formation times were also noted, which are expected since less NO_x was stored during the previous lean phase for Pt-Ba/Al-Ti and Pt-Ba/Al-Ti_{MF}. N_2 production was still immediate after switching to rich conditions over these catalysts as well, indicating rapid nitrite/nitrate reduction. NH_3 was not detected for Pt-Ba/Al-Ti. For the physical mixture, Pt-Ba/Al-Ti_{MF}, the amount of NH_3 was ca. 25 ppm and was smaller than that obtained over the Pt-Ba/Al_{NF} catalyst, which was ca. 95 ppm. NH_3 is formed via a reaction between the surface NO_x species and the entering H_2. Since less NO_x was trapped on the Pt-Ba/Al-Ti and Pt-Ba/Al-Ti_{MF} samples, less NH_3 will ultimately be generated and due to the small amount of NO_x trapped on Pt-Ba/Al-Ti, none was observed. The nanofiber-supported sample led to less NH_3 generation, although more NO_x was trapped, demonstrating better selectivity toward N_2 formation.

In Fig. 5 the performance at different temperatures are shown for the Pt-Ba_{ST}, Pt-Ba/Al_{NF}, and Pt-Ba/Al-Ti catalysts. For all studied materials, NO to NO_2 oxidation increased with increasing reaction temperature (data listed in Table 2). This increase in oxidation capacity is especially obvious when comparing the Pt-Ba_{ST} and Pt-Ba/Al_{NF} performance at 523 and 623 K.

For standard Pt-Ba_{ST}, the trapping efficiency increased between 523 and 623 K. At higher temperatures, the amount of NO_x stored slightly decreased and starting at 623 K, NO_x release at the onset of the rich phase was observed, indicating that the nitrites/nitrates stability became significant. It has been proposed that the NO_x released at the onset of regeneration can be related to heat generation during oxidation of the reductant species, if enough reductant is present (thermal release) [48,49] and/or the thermodynamic stability of nitrates, which decreases in a net reducing environment [50]. Ammonia production was highest at 523 K, ca. 280 ppm was the peak amount, and its formation decreased as reaction temperature increased, which is consistent with the literature [48,51]. The amount of NO_x trapped over the Pt-Ba/Al_{NF} catalyst is higher at all temperatures tested compared to the Pt-Ba_{ST} standard catalyst. Moreover, there was no evidence of NO_x release at the onset of, or any time during, the rich phase. Also the amount of NH_3 produced is consistently lower relative to that made over the standard Pt-Ba_{ST}. For example, at 523 K the amount of NH_3 formed over the Pt-Ba/Al_{NF} catalyst is ca. 40% lower than that obtained with Pt-Ba_{ST}. As with Pt-Ba_{ST}, NH_3 formation over Pt-Ba/Al_{NF} decreased with temperature. These results are in line with literature data, where decreased NH_3 formation with increasing temperature has been related to lower nitrite/nitrate species stability, such that the released NO_x:reductant ratio is too high for substantial NH_3 formation. Also, taking into account NO- or N-species adsorbed onto Pt reacting with H_2, more NH_3 would form during regeneration at

Table 2
NO_2 concentration at the end of the lean phase (1000 ppm NO_x + 3% O_2 in He).

Temperature (K)	NO_2 out (ppm)			
	Pt-Ba_{ST}	Pt-Ba/Al_{NF}	Pt-Ba/Al-Ti	Pt-Ba/Al-Ti_{MF}
RT	<10	<10	<10	<10
523	35	45	20	35
623	320 (60)	390 (75)	45 (<10)	160 (35)
723	320	350	65	170
773	320	340	80	155

() in brackets – NO_2 out ppm in the presence of H_2O and CO_2 during TRM. Both lean and rich phases contained 2.5% H_2O and 5% CO_2.

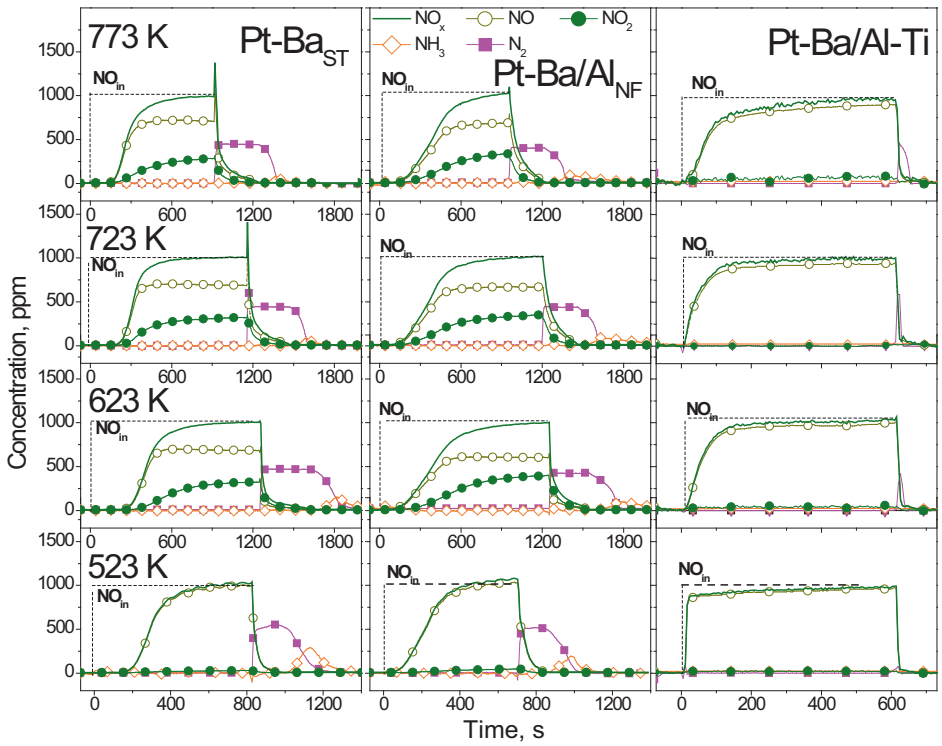

Fig. 5. NO_x concentration profiles at different temperatures. Lean phase – 1000 ppm NO + 3% O_2 in He; regeneration phase – 2000 ppm H_2 in He. Gas flow = 100 ml min^{-1}.

lower temperature because more NO_x species are available over a longer period of time due to slower diffusion rates between the nitrate sites and Pt. Additionally, the ratio of H_2 fed to NO_x stored has an important effect on selectivity to N_2 and NH_3 [48,51]. For Pt-Ba/Al-Ti, the trapping efficiency at 523 K is poor. The amount of NO_x trapped increased with temperature, at least up to 773 K. During the rich phase, no NO_x release was detected and NH_3 was produced only at 523 K, and was less than 10 ppm at its peak, due to the small amount of NO_x trapped.

The TRM data demonstrate that the addition of Ti to the support significantly influences the general NO_x storage and reduction behaviour, significantly decreasing the storage capacity and therefore resulting in poorer performance. The Pt-Ba/Al_{NF} catalyst has better performance than the other catalysts in terms of NO_x removal at all temperatures evaluated.

The good Pt dispersion obtained for the Pt-Ba/Al_{NF} system implies closer proximity of Pt to the storage components. The beneficial influence of such a proximal configuration on NO_x storage has been described elsewhere [12,13]. Additionally, Pt-Ba/Al_{NF} has a higher Pt and Ba exposed amount than Pt-Ba/Al-Ti and Pt-Ba_{ST} (Table 1). For Pt-Ba/Al_{NF}, BaO or $Ba(OH)_2$ are probably the most abundant storage species. $BaCO_3$ was almost negligible (small XRD features, no CO_2 evolved during regeneration), because this phase was likely decomposed during catalyst conditioning. In the case of Pt-Ba/Al-Ti, BaO or $Ba(OH)_2$ are still likely storage species at temperatures below 873 K, due to the absence of CO_2 evolved during reaction. When exposing Pt-Ba/Al-Ti to higher temperatures (873–1223 K), Ba-Ti complex structures can form, such as $Ba_xTi_yO_z$, and/or $Ba_xAl_yTi_zO_n$, and this interaction can play an important role [39]. It was previously found for ternary oxides, that the TiO_2 domains have a significant affinity toward BaO and/or $Ba(NO_3)_2$ resulting in strong Ti-Ba interactions and the formation of overlapping domains on the surface [39]. The presence of Ti can also induce a decrease in the decomposition temperature of the $Ba(NO_3)_2$ phase with respect to the Ti-free $Ba(NO_3)_2/\gamma$-Al_2O_3 system. Such a destabilization was attributed to a weaker interaction between $Ba(NO_3)_2$ and γ-Al_2O_3 domains in the ternary oxide as well as due to the change in the surface acidity in the presence of TiO_2 [39]. It was also previously reported that Ti domains provide strong anchoring sites for the Ba-containing units and significantly alter the surface morphology, composition and the stoichiometry of the Ba-containing units as well as the surface mobility of the BaO clusters [52]. In this study, the formation of complex Ba-Al-Ti-O structures was not observed via XRD at temperatures below 873 K and because of that the Pt-Ba/Al-Ti system had some NO_x storage capacity through the tested temperature range. However, the XRD data indicate that Pt-Ba/Al-Ti seems to have interesting properties from the point of view of thermal durability. The pure Al-Ti nanofibrous support is stable up to ca. 1200 K and when impregnated with Pt and Ba, doesn't show significant textural changes up to ca. 900 K. Although the catalyst supported Al-Ti nanofiber had a lower BET surface area compared with pure Al_{NF}, it partially preserves its porous structure even after the thermal treatment at ca. 1200 K.

In Fig. 6 the TPD profiles of stored nitrite/nitrate decomposition products are shown. The temperatures where a desorption maximum occurred for each catalyst are listed in Table 3. Note, the sharp increase noted at approximately 2100 and 2000 s in the 2nd and bottom plots are due to instrument data acquisition speed "missing" the transition to the increased concentration value. The

Table 3
Desorption temperatures of N- and S-species (sh – shoulder).

Catalyst	Nitrates desorption temperature (K)	Desulfurization temperature (K)
Pt-Ba_{ST}	590 (sh), 620, 670 (sh)	777 (sh), 873, 930_{SO2}
Pt-Ba/Al_{NF}	570 (sh), 639, 695 (sh)	730 (sh), 812, 910
Pt-Ba/Al-Ti	609 (sh), 650, 730 (sh)	730 (sh), 850
Pt-Ba/Al-Ti_{MF}	570 (sh), 649, 715 (sh)	730 (sh), 830, 910

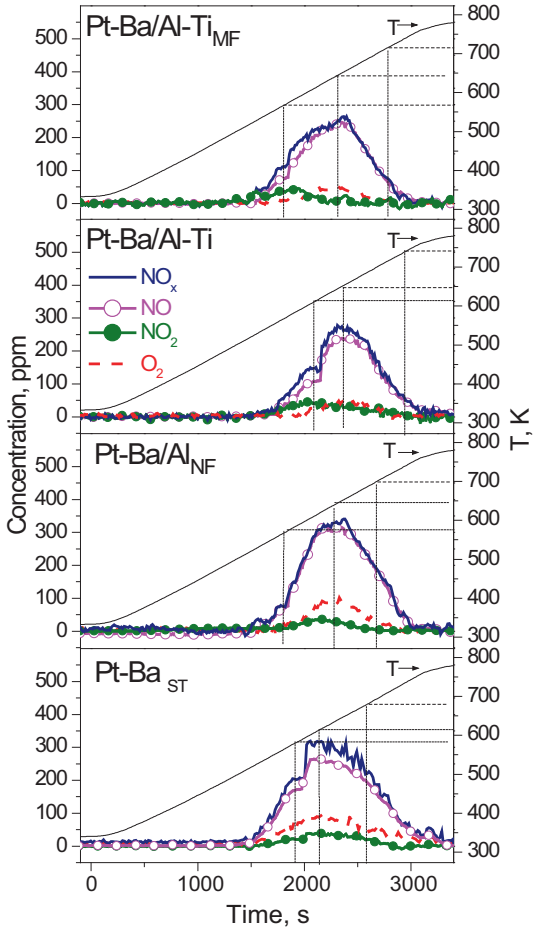

Fig. 6. He TPD after a lean phase of a TRM experiment. Heating rate = 10 K min^{-1}. Gas flow = 100 ml min^{-1}.

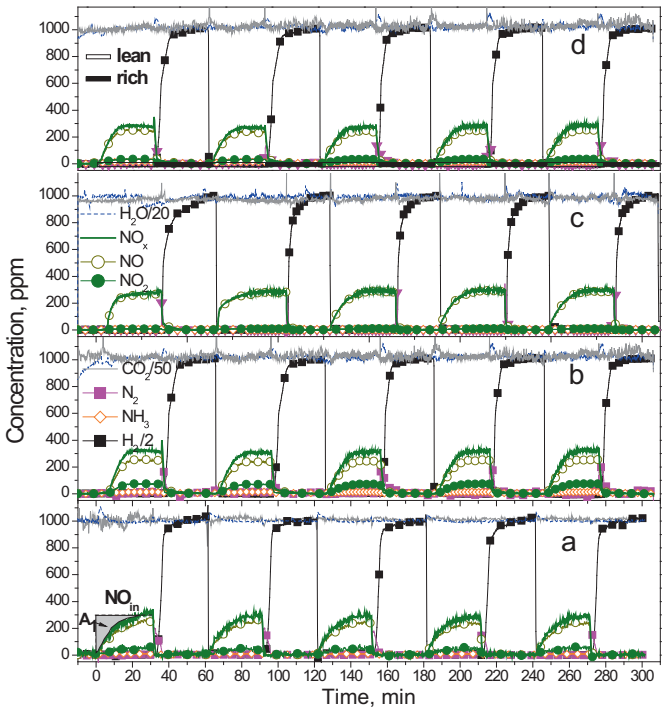

Fig. 7. Water and CO_2 influence on NO_x storage–reduction at 623 K for (a) Pt-Ba$_{ST}$, (b) Pt-Ba/Al$_{NF}$, (c) Pt-Ba/Al-Ti and (d) the physical mixture of Pt-Ba/Al-Ti$_{MF}$. Lean phase – 300 ppm NO_x + 3% O_2 in He; regeneration phase – 2000 ppm H_2 in He. Each phase contained 2.5% H_2O and 5% CO_2. Gas flow = 100 ml min^{-1}.

thermal evolution of the stored NO_x species on the surface of Pt-Ba/Al$_{NF}$ shows one major desorption feature with two shoulders. The NO_x desorption maximum is at 639 K and the first shoulder is ca. 570 K while the second small shoulder is observed at 695 K. The desorption features observed above 600 K are associated most probably with the decomposition of bridging and bidentate nitrates [52]. Although the thermal stabilities of the sorbed NO_x species are similar for Pt-Ba$_{ST}$ and Pt-Ba/Al$_{NF}$, there was no release of unreduced NO_x observed for Pt-Ba/Al$_{NF}$, indicating that the reduction process over Pt-Ba/Al$_{NF}$ is more efficient, likely due to the better dispersion obtained with the higher initial surface area.

The thermal stability of the adsorbed NO_x species was found to be in good agreement with literature. Previous studies indicate that the presence of TiO_2 (rutile) crystallites on the surface of the alumina particles significantly influence the nature of the adsorbed NO_x species by providing additional Ti^{4+} NO_x storage sites [52]. The large TiO_2 crystallites can partially block some of the accessible Al^{3+} surface sites. Moreover, the BaO domains possess a lower surface area [52]. A lower temperature feature at 389 K, related to the desorption of weakly bound N_2O_3 and NO^+ species that desorb in the form of NO_2 and NO + O_2 [52], was not observed during this study. This peak has been attributed to the N-species stored on the alumina support. Its absence is likely due to the alumina surface of Pt-Ba/Al$_{NF}$ and Pt-Ba/Al-Ti being partially blocked.

For the Pt-Ba/Al-Ti catalyst, all the desorption features are at higher temperatures relative to the other catalysts. The high temperature desorption feature, the shoulder at ca. 730 K, can be assigned to the decomposition of the bulk Ba-nitrates and nitrate species associated with Ti [52]. Evidence from a previous study also shows a peak at ca. 900–930 K, which is due to decomposition of Ba-nitrates located on the surface of TiO_2 [52]. Both of these nitrate species decompose by releasing mostly NO. According to this previous study, this thermal stabilization of the bulk Ba-nitrates and their decomposition at higher temperatures can be explained by the stronger interaction between the bulk BaO domains and the underlying Ti sites, where large BaO clusters are immobilized on the TiO_2/TiO_x domains, and apparently the Ti stabilizes the other features as well.

3.3. H_2O and CO_2 influence

The influence of H_2O and CO_2 on the Pt-Ba$_{ST}$, Pt-Ba/Al$_{NF}$, Pt-Ba/Al-Ti and Pt-Ba/Al-Ti$_{MF}$ catalysts' behaviour was investigated and results obtained at 623 K are presented in Fig. 7. Compared to "clean" conditions (without H_2O and CO_2), Fig. 4, the NO_x breakthrough time is shorter in the presence of H_2O and CO_2, indicating that NO_x is stored more efficiently in the absence of both H_2O and CO_2. This is in good agreement with previous studies, where the combined effect of H_2O and CO_2 on the storage of Pt/Ba/Al_2O_3 catalysts has been investigated [53–55]. For Pt-Ba$_{ST}$ the total uptake of NO_x time is ca. 0.7 min for "clean" conditions, while in the presence of H_2O and CO_2 it decreases to ca. 0.4 min. Additionally, the NO oxidation activity is influenced and at the end of the lean phase the amount of NO_2 was ca. 60-70 ppm (Table 2). A smaller effect on catalytic activity was observed for the Pt-Ba/Al$_{NF}$, where the amount of NO_x stored decreased by ca. 28% compared to the amount trapped in the absence of H_2O and CO_2. A partial loss of NO oxidation activity for this catalyst was also detected. In general, the decrease in catalytic activity due to H_2O and CO_2 presence is: Pt-Ba$_{ST}$ > Pt-Ba/Al-Ti > Pt-Ba/Al-Ti$_{MF}$ > Pt-Ba/Al$_{NF}$. It is worth noting that at 623 K, NH_3 formation was not observed during the rich phase, which is consistent with previous findings, where it was suggested that CO_2

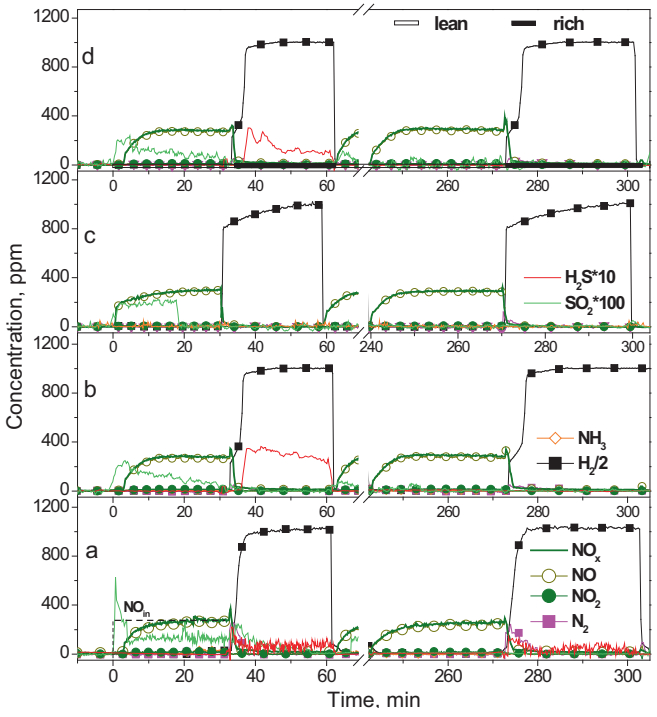

Fig. 8. NO_x storage–reduction at 623 K for sulfated catalysts (first and last TRM cycle); (a) Pt-Ba_{ST}, (b) Pt-Ba/Al_{NF}, (c) Pt-Ba/Al-Ti and (d) the physical mixture of Pt-Ba/Al-Ti_{MF}. Lean phase – 1000 ppm NO_x + 3% O_2 in He; regeneration phase – 2000 ppm H_2 in He. Each phase contained 2.5% H_2O and 5% CO_2. Gas flow = 100 ml min^{-1}.

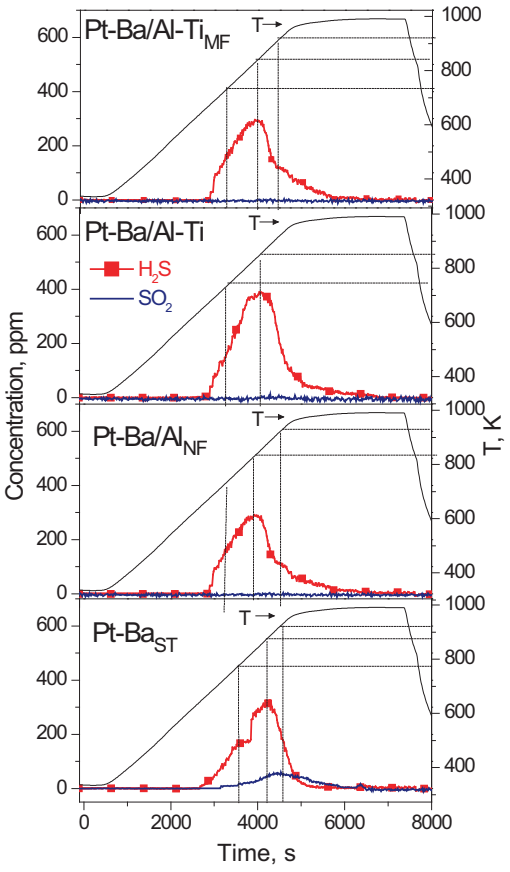

Fig. 9. TPR/desulfurization with 2000 ppm H_2 + 2.5% H_2O + 5% CO_2 in He. Total flow = 100 ml min^{-1}. *T* ramp = 10 K min^{-1}.

has a promoting effect on NH_3 formation only at low temperatures (lower than 573 K) [55].

Previous studies have shown that in the presence of H_2O and CO_2, hydroxide and carbonate catalyst storage species are formed [56–58]. Therefore, the proposed explanation for the lower storage capacity in the presence of H_2O and CO_2 is that NO_x storage is more difficult on $BaCO_3$ and $Ba(OH)_2$ than on BaO [55]. It has also been shown that CO_2 has a greater influence on storage relative to H_2O [55], which was related to the greater stability of $BaCO_3$ compared to $Ba(OH)_2$, resulting in more difficult nitrite/nitrate formation from $BaCO_3$.

3.4. Sulfur poisoning study

The effects of the nanofibrous support structure and Ti incorporation in the Al phase on sulfur adsorption suppression, and NO_x storage afterwards, were studied over the Pt-Ba/Al_{NF}, Pt-Ba/Al-Ti and Pt-Ba/Al-Ti_{MF} catalysts, and the results were compared with those obtained from the standard Pt-Ba catalyst. All performance tests of the S-poisoned and desulfurized catalysts were performed in the presence of 2.5% H_2O and 5% CO_2, except the sulfation portion itself, as both of these compounds can promote desulfurization [59]. The storage–reduction profiles at 623 K after sulfation are shown in Fig. 8. The results clearly show that after sulfation, the first adsorption–reduction cycle is significantly perturbed relative to those shown in Figure 7. During the first adsorption phase, SO_2 was released from all samples, whereas H_2S formation was observed during the first regeneration phase for the Pt-Ba/Al_{NF} and Pt-Ba/Al-Ti_{MF} catalysts. For all catalysts, NO_x removal activity decreased compared to the corresponding un-sulfated systems. The NO breakthrough time dropped 48-67% and the NO to NO_2 oxidation extents were also inhibited. The NO_x conversion over all of the sulfated catalysts increased slowly with time (number of cycles), which indicates that the catalyst active centres can be to some extent recuperated at 623 K under normal, cycling conditions. However, there is only a moderate level of activity re-attained after 300 min or after 5 cycles. The amounts of stored nitrates at 623 K for sulfated Pt-Ba_{ST}, Pt-Ba/Al_{NF} and Pt-Ba/Al-Ti were 5.08×10^{-4}, 7.69×10^{-4} and 5.67×10^{-4} mol g_{cat}^{-1}, respectively, and are all slightly higher than previously reported values for a standard Pt/Ba/Al_2O_3 catalyst [50].

Moreover, a small release of unconverted NO_x at the onset of regeneration for all sulfated catalysts was detected. The highest amount of unconverted NO_x was released from the standard Pt-Ba_{ST}. The highest decrease in overall activity, ca. 37% was obtained from the standard catalyst as well. The Ti-modified catalysts actually perform better than the standard after this S exposure. This could be due to Ba sites associated with Ti being affected less significantly than Ba not associated with Ti.

The data obtained during the TPR used for desulfurization are shown in Fig. 9 and temperatures where a S-species desorption maximum occurred for each catalyst are given in Table 3. H_2 was used as the reducing agent, and is known to promote sulfur desorption [3]. The temperature for the onset of S release was similar for each catalyst. For the sulfated Pt-Ba_{ST} standard catalyst, H_2S and SO_2 are both observed, with maxima in desorption noted at ca. 773 and 873 K for H_2S and 930 K for SO_2. Sulfur removal can be explained on the basis of reactions (1) and (2) or reaction (1) with the product SO_2 further reacting with H_2 to form H_2S.

$$BaSO_4 + H_2 \rightarrow BaO + SO_2 + H_2O \quad (1)$$

$$BaSO_4 + 4H_2 \rightarrow BaO + H_2S + 3H_2O \quad (2)$$

Pt promotes both reactions and lowers the desorption temperature [3].

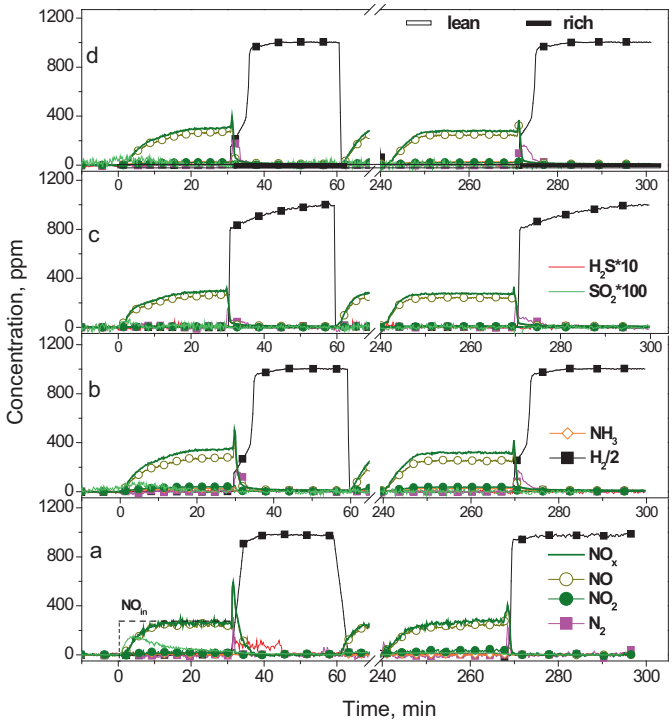

Fig. 10. TRM profiles at 623 K for the desulfurized catalysts (first and last TRM cycle); (a) Pt-Ba_{ST}, (b) Pt-Ba/Al_{NF}, (c) Pt-Ba/Al-Ti and (d) the physical mixture of Pt-Ba/Al-Ti_{MF}. Lean phase – 1000 ppm NO_x + 3% O_2 in He; regeneration phase – 2000 ppm H_2 in He. Each phase contained 2.5% H_2O and 5% CO_2. NO_x = NO + NO_2. Gas flow 100 ml min^{-1}.

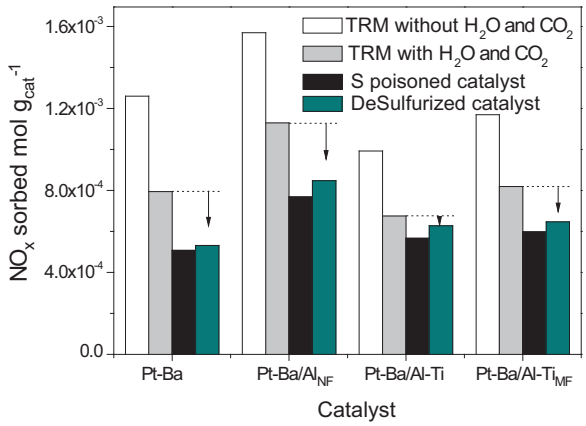

Fig. 11. NO_x storage over fresh (with and without H_2O and CO_2), sulfated and desulfurized catalysts.

Table 4
Catalyst activity recovery after sulfation and desulfurizarion (A_{DES}) in H_2.

Catalyst	A_{DES}	A_{DES^*}
Pt-Ba_{ST}	0.97	0.92
Pt-Ba/Al_{NF}	0.90	0.78
Pt-Ba/Al-Ti	0.86	0.44
Pt-Ba/Al-Ti_{MF}	0.91	0.78

$A_{DES} = (NO_{ads} - NO_{ads\ DES})/(NO_{ads} - NO_{ads\ SULF})$, $A_{DES^*} = (NO_{ads^*} - NO_{ads\ DES})/(NO_{ads^*} - NO_{ads\ SULF})$, where NO_{ads} – amount NO adsorbed during TRM at 623 K under 'clean' conditions, NO_{ads^*} – amount NO adsorbed during TRM at 623 K with CO_2 and H_2O added, $NO_{ads\ DES}$ – amount NO adsorbed over desulfurized catalyst during TRM at 623 K with CO_2 and H_2O added, $NO_{ads\ SULF}$ – amount NO adsorbed over sulfated catalyst during TRM at 623 K with CO_2 and H_2O added.

Significant SO_2 formation was observed only for Pt-Ba_{ST}. For the nanofibrous material, H_2S desorption was predominant at temperatures above 673 K and SO_2 formation was negligible, less than 5 ppm. For the Pt-Ba/Al-Ti catalyst, the amount of H_2S desorbed was noticeably higher than that from the other catalysts investigated. This indicates that Ti incorporation into the alumina nanofiber structure either results in more S adsorbed during the sulfation process or catalyzes the release of S as H_2S. TiO_2 is known to be resistant to sulfur poisoning, because sulfates on TiO_2 are less stable than those on other oxides, such as γ-Al_2O_3 [24,25,39], possibly due to acidity differences [[25] and references therein] or the interaction between the Ti and Ba, forming overlapping domains as discussed above [50]. This better sulfur tolerance was also observed previously for TiO_2 supports and TiO_2 mixed with γ-Al_2O_3 [3,7] and it has been reported that Pt/TiO_2 mixed with Pt-Ba/Al_2O_3 shifts sulfur desorption to lower temperatures. Additionally, H_2S desorbs more easily at lower temperature in the vicinity of the interface where Pt/TiO_2 and sulfur poisoned Pt-Ba/Al_2O_3 are in contact [7]. This facilitation of sulfur desorption is therefore a function of an increase in interfacial contact between Al_2O_3 and TiO_2 [7]. Accordingly, the prepared nanofibrous material containing Ti seemingly results in high contact between the two interfaces and it is the release of S that is increased.

In Fig. 10, the TRM profiles obtained after desulfurization are displayed. The first lean-rich TRM cycle was significantly changed for all cases. For the desulfurized catalysts, the NO breakthrough time is higher and the amount of NO_x stored increased compared to the corresponding sulfated systems. Also, the NO to NO_2 oxidation ability improved after desulfurization, by 15-20%. The total amounts of NO_x stored before and after sulfation as well as after desulfurization for each catalyst are shown in Fig. 11. The N balances are within 4–7%. The best performance after desulfurization was obtained for the nanofibrous Pt-Ba/Al_{NF} and Pt-Ba/Al-Ti systems (data listed in Table 4).

Interestingly, SO_2 and H_2S were still observed being released over the previously desulfurized catalysts (Fig. 10). SO_2 release during the storage phase is observed mostly for Ti-free systems, indicating that some residual S-species are present on the Pt-Ba_{ST} and Pt-Ba/Al_{NF} catalyst surfaces after desulfurization and that the added NO_x and O_2 presumably induces some release that did not occur under the reducing TPR conditions. In this context, Ti presumably increases sulfur desorption, which is in agreement with the data discussed above as well as previous work [7]. However, there is also a noticeable increase in unconverted NO_x release after the TPR protocol. After desulfurization the highest amount of unconverted NO_x was released with Pt-Ba_{ST} (1.42×10^{-6} mol g_{cat}^{-1}) and Pt-Ba/Al_{NF} resulted in less (2.84×10^{-7} mol g_{cat}^{-1}), but more than prior to the TPR. Moreover, for those catalysts, the highest decrease in overall activity is obtained, i.e. 33 and 25% for Pt-Ba_{ST} and Pt-Ba/Al_{NF}, respectively. For Pt-Ba/Al-Ti, the amount of unconverted NO_x is almost negligible (5.61×10^{-8} mol g_{cat}^{-1}) and for Pt-Ba/Al-Ti_{MF} the amount of unconverted NO_x (1.09×10^{-7} mol g_{cat}^{-1}) falls between those obtained for Pt-Ba/Al_{NF} and Pt-Ba/Al-Ti. H_2S release was observed during the rich phase for Pt-Ba_{ST} in the first TRM cycle, but was not for the other catalysts.

The NO_x storage–reduction tests with the desulfurized catalysts reveal that the NO_x storage capacity was higher for the nanofibrous alumina and Al-Ti supported catalysts compared to standard Pt-Ba, further suggesting that sulfur desorption was promoted over those catalysts, resulting in better recovered performance.

4. Conclusions

Different NO_x storage catalysts deposited on nanofibrous supports were prepared, with comparison also made to a model NSR catalyst. The modification of the nanofibrous γ-Al_2O_3 structure by Ti negatively affected NO_x storage properties but enhanced the

thermal durability and S resistance. NO_x storage increased with temperature, up to 773 K with the addition of Ti, while for the other samples, trapping ability decreased at this high temperature relative to lower temperatures. This was due to the availability of additional NO_x adsorption sites associated with the Ti or Ba/Ti interactions. The Pt-Ba catalyst supported on pure nanofibrous γ-Al_2O_3 had the best results at temperatures below 723 K. This sample also resulted in the best NO oxidation performance, likely leading to the improved trapping ability, although its better dispersion of both Pt and Ba sites also leads to improved performance. S exposure affected both NO_x storage and unconverted NO_x release during the regeneration phase. The Ti-modified sample released more sulfur during TPR than the others indicating enhanced contact between Al_2O_3 and TiO_2.

Acknowledgments

The authors wish to thank the Spanish Ministry of Education (MEC) for the FPI grant, projects CTQ2006-09780 and CTQ2009-10649 and Canada Foundation for Innovation for the equipment grant.

Appendix A. Supplementary data

Supplementary data associated with this article can be found, in the online version, at doi:10.1016/j.cattod.2011.02.045.

References

[1] Y. Huang, Q. Lu, SAE Technical Paper 24-0103 (2007).
[2] J.H. Kwak, D.H. Kim, J. Szanyi, C.H.F. Peden, Appl. Catal. B 84 (2008) 545.
[3] S. Matsumoto, Y. Ikeda, H. Suzuki, M. Ogai, N. Miyoshi, Appl. Catal. B 25 (2000) 115.
[4] W. Muller, W. Strehlau, J. Hoehne, A. Okumura, U. Gobel, E. Lox, M. Hori, SAE Technical Paper 01-1285 (1999).
[5] F. Rohr, I. Grisstede, A. Sundararajan, W. Mueller, SAE Technical Paper 01-0766 (2008).
[6] E. Schreier, R. Eckelt, M. Richter, R. Fricke, Appl. Catal. B (2006) 249.
[7] H. Hirata, I. Hachisuka, Y. Ikeda, S. Tsuji, S. Matsumoto, Top. Catal. 16/17 (2001) 145.
[8] K. Yamazaki, T. Suzuki, N. Takahashi, K. Yokota, M. Sugiura, Appl. Catal. B 30 (2001) 459.
[9] J.A. Anderson, Z. Liu, M.F. Garcia, Catal. Today 113 (2006) 25.
[10] P. Forzatti, L. Lietti, Catal. Today 155 (2010) 131.
[11] L. Lietti, P. Forzatti, I. Nova, E. Tronconi, J. Catal. 204 (2001) 175.
[12] I.S. Pieta, M. García-Diéguez, M.C. Herrera, M.A. Larrubia, L.J. Alemany, J. Catal. 270 (2010) 256.
[13] W.S. Epling, L.E. Campbell, A. Yezerets, N.W. Currier, J.E. Parks, Catal. Rev. 46 (2004) 163.
[14] E. Fridell, M. Skoglundh, B. Westerberg, S. Johansson, G. Smedler, J. Catal. 183 (1999) 196.
[15] M. Molinier, SAE Technical Paper 01-0508 (2001).
[16] N. Takahashi, K. Yamazaki, H. Sobukawa, H. Shinjoh, Appl. Catal. B 170 (2007) 198.
[17] M. Takeuchi, S. Matsumoto, Top. Catal. 28 (2004) 151.
[18] J.P. Day, W. Cutler, SAE Technical Paper 01-3500 (1999).
[19] J.R. Theis, J.J. Li, R.G. Hurley, J.A. Ura, SAE Technical Paper 01-0733 (2002).
[20] D.H. Kim, Y.H. Chin, G.G. Muntean, A. Yezeretz, N.W. Currier, W.S. Epling, H.Y. Chen, H. Hess, C.H.F. Peden, Ind. Eng. Chem. Res. 45 (2006) 8815.
[21] S. Matsumoto, Catal. Today 90 (2004) 183.
[22] G.A. Ingram, G. Surnilla, SAE Technical Paper 01-0731 (2002).
[23] W.E.J.v. Kooten, H.C. Krijnsen, C.M.v.d. Bleek, H.P.A. Calis, Appl. Catal. B 25 (2000) 125.
[24] H. Mahzoul, P. Gilot, J.-F. Brilhac, B.R. Stanmore, Top. Catal. 16/17 (2001) 293.
[25] K. Yamamoto, R. Kikuch, T. Takeguchi, K. Eguch, J. Catal. 238 (2006).
[26] Q. Wang, J.H. Sohn, J.S. Chunk, Appl. Catal. B 89 (2009) 97.
[27] D.H. Kim, Y.H. Chin, J.H. Kwak, J. Szanyi, C.H.F. Peden, Catal. Lett. 105 (2005) 259.
[28] T. Szailer, J.H. Kwak, D.H. Kim, J. Szanyi, C.M. Wang, C.H.F. Peden, Catal. Today 114 (2006) 86.
[29] Q. Wang, J.S. Chung, Appl. Catal. A 358 (2009) 59.
[30] N. Takahashi, S. Matsunaga, T. Tanaka, H. Sobukawa, H. Shinjoh, Appl. Catal. B 77 (2007) 73.
[31] I. Hachisuka, T. Yoshida, H. Ueno, N. Takahashi, A. Suda, M. Sugiura, SAE Technical Paper 01-0732 (2002).
[32] M. García-Diéguez, I.S. Pieta, M.C. Herrera, M.A. Larrubia, I. Malpartida, L.J. Alemany, Catal. Today 149 (2010) 380.
[33] Z. Zhu, H. Liu, H. Sun, D. Yang, Microporous Mesoporous Mater. 123 (2009) 39.
[34] J. Dawody, L. Eurenius, H. Abdulhamid, M. Skoglundh, E. Olsson, E. Fridell, Appl. Catal. A 296 (2005) 157.
[35] J.H. Kwak, D. Mei, C.W.W. Yi, D.H. Kim, C.F. Peden, L. Allard, J. Szanyi, J. Catal. 261 (2009) 17.
[36] D. Mei, Q. Ge, J.H. Kwak, D.H. Kim, J. Szanyi, C.F. Peden, J. Phys. Chem. C 112 (2008) 18050.
[37] M. Piacentini, M. Maciejewski, A. Baiker, Appl. Catal. B 60 (2005) 265.
[38] C.L.M. Scholz, B.H.W. Maes, M.H.J.M.d. Croon, J.C. Schouten, Appl. Catal. A 332 (2007) 1.
[39] S.M. Andonova, G.S. Senturk, E. Kayhan, E. Ozensoy, J. Phys. Chem. C 113 (2009) 11014.
[40] J.A. Anderson, B. Bachiller-Baeza, M. Fernandez-Garcia, Phys. Chem. Chem. Phys. 20 (2003) 4418.
[41] H. Mahzoul, J.F. Brilhac, P. Gilot, Appl. Catal. B 20 (1999) 47.
[42] H.Y. Huang, R.Q. Long, R.T. Yang, Energy Fuel 15 (2001) 205.
[43] F. Prinetto, G. Ghiotti, I. Nova, L. Lietti, E. Tronconi, P. Forzatti, J. Phys. Chem. B 105 (2001) 12732.
[44] L. Li, Q. Shen, J. Cheng, Z. Hao, Appl. Catal. B 93 (2010) 259.
[45] Y. Xu, W.A. Shelton, W.F. Schneider, J. Phys. Chem. A 110 (2006) 5839.
[46] S. Decker, K.J. Klabunde, JACS 118 (1996) 12465.
[47] J.Y. Luo, M. Meng, Y.Q. Zha, Y. Ning, T.D. Hu, J. Zhang, T. Liu, Appl. Catal. B 78 (2008) 38.
[48] W.S. Epling, A. Yezerets, N.W. Currier, Appl. Catal. B 74 (2007) 117.
[49] K.S. Kabin, R.L. Muncrief, M.P. Harold, Catal. Today 96 (2004) 79.
[50] Z. Liu, J.A. Anderson, J. Catal. 224 (2004) 18.
[51] P. Forzatti, L. Lietti, N. Gabrielli, Appl. Catal. B 99 (2010) 145.
[52] S.M. Andonova, G.S. Senturk, E. Ozensoy, J. Phys. Chem. C 114 (2010) 17003.
[53] W.S. Epling, G.C. Campbell, J.E. Parks, Catal. Lett. 90 (2003) 45.
[54] W.S. Epling, J.E. Parks, G.C. Campbell, A. Yezerets, N.W. Currier, L.E. Campbell, Catal. Today (2004) 21.
[55] A. Lindholm, N.W. Currier, E. Fridell, A. Yezerets, L. Olsson, Appl. Catal. B 75 (2007) 78.
[56] S. Balcon, C. Potvin, L. Salin, J.F. Tempere, G. Djega-Mariadassou, Catal. Lett. 60 (1999) 39.
[57] F. Rodrigues, L. Juste, C. Potvin, J.F. Tempere, G. Blanchard, G. Djega-Mariadassou, Catal. Lett. 72 (2001) 59.
[58] T.J. Toops, D.B. Smith, W.S. Epling, J.E. Parks, W.P. Partridge, Appl. Catal. B 58 (2005) 255.
[59] D.H. Kim, J.H. Kwak, J. Szanyi, X. Wang, M.H. Engelhard, C.H.F. Peden, Top. Catal. 52 (2009) 1719.